Journal Pre-proof

Frataxin inhibits the sensitivity of the myocardium to ferroptosis by regulating iron homeostasis

Zhang Zihui, Wenhua Jiang, Chan Zhang, Yue Yin, Nan Mu, Yishi Wang, Lu Yu, Heng Ma

PII: S0891-5849(23)00503-8

DOI: https://doi.org/10.1016/j.freeradbiomed.2023.06.016

Reference: FRB 16073

To appear in: *Free Radical Biology and Medicine*

Received Date: 4 May 2023

Revised Date: 8 June 2023

Accepted Date: 19 June 2023

Please cite this article as: Z. Zihui, W. Jiang, C. Zhang, Y. Yin, N. Mu, Y. Wang, L. Yu, H. Ma, Frataxin inhibits the sensitivity of the myocardium to ferroptosis by regulating iron homeostasis, *Free Radical Biology and Medicine* (2023), doi: https://doi.org/10.1016/j.freeradbiomed.2023.06.016.

Frataxin inhibits the sensitivity of the myocardium to ferroptosis by regulating iron homeostasis

Zihui Zhang[1#], Wenhua Jiang[1#], Chan Zhang[1], Yue Yin[2], Nan Mu[2], Yishi Wang[2], Lu Yu[3,*], Heng Ma[2,*]

[1]Institute of Medical Research, Northwestern Polytechnical University, Xi'an Shaanxi, 710072, P.R. China

[2] Department of Physiology and Pathophysiology, School of Basic Medicine, Fourth Military Medical University, Xi'an Shaanxi, 710032, P.R. China

[3] Department of Pathology, Xijing Hospital, Fourth Military Medical University, Xi'an, China.

[#]Zihui Zhang and Wenhua Jiang contributed equally.

*** Correspondence:**

Heng Ma, M.D., Ph.D.
Department of Physiology and Pathophysiology, School of Basic Medical Sciences, Fourth Military Medical University, Xi'an 710032, China. E-mail: hengma@fmmu.edu.cn;

&

Lu Yu, M.D., Ph.D.
Department of Pathology, Xijing Hospital, Fourth Military Medical University, Xi'an, 710032, China. Email: yulu@fmmu.edu.cn

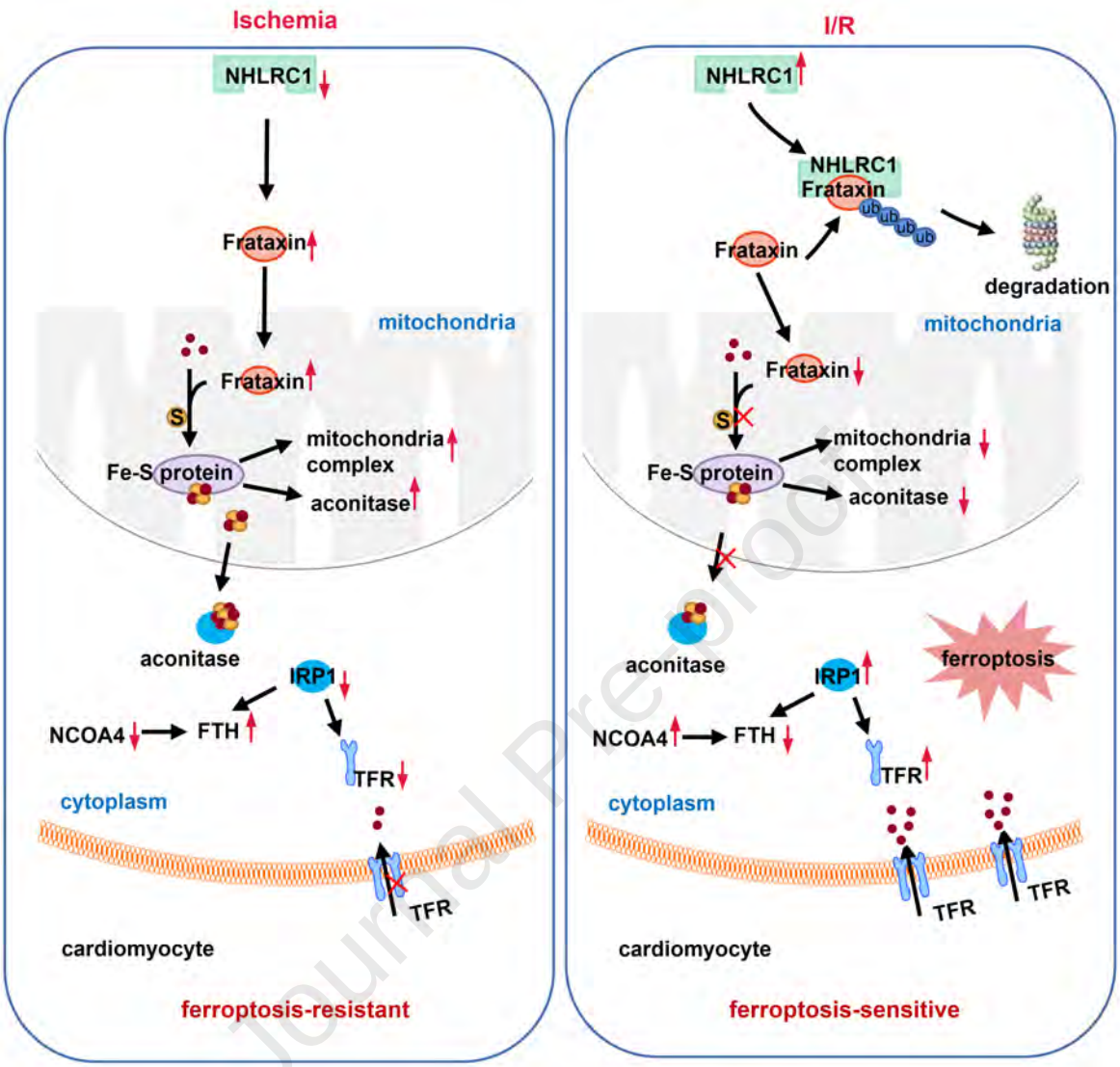

Frataxin inhibits the sensitivity of the myocardium to ferroptosis by regulating iron homeostasis

Zihui Zhang[1#], Wenhua Jiang[1#], Chan Zhang[1], Yue Yin[2], Nan Mu[2], Yishi Wang[2], Lu Yu[3,*], Heng Ma[2,*]

[1]Institute of Medical Research, Northwestern Polytechnical University, Xi'an Shaanxi, 710072, P.R. China

[2] Department of Physiology and Pathophysiology, School of Basic Medicine, Fourth Military Medical University, Xi'an Shaanxi, 710032, P.R. China

[3] Department of Pathology, Xijing Hospital, Fourth Military Medical University, Xi'an, China.

[#]Zihui Zhang and Wenhua Jiang contributed equally.

*** Correspondence:**

Heng Ma, M.D., Ph.D.
Department of Physiology and Pathophysiology, School of Basic Medical Sciences, Fourth Military Medical University, Xi'an 710032, China. E-mail: hengma@fmmu.edu.cn;

&

Lu Yu, M.D., Ph.D.
Department of Pathology, Xijing Hospital, Fourth Military Medical University, Xi'an, 710032, China. Email: yulu@fmmu.edu.cn

Highlights

- IRP activity was enhanced in ischemic hearts and weakened in reperfused hearts.
- NHLRC1 promoted frataxin ubiquitination and degradation.
- Cardiac-specific frataxin overexpression protected against myocardial I/R injury through ferroptosis inhibition.

Abstract

Rationale: Myocardial ischemia/reperfusion (I/R) injury is characterized by cell death via various cellular mechanisms upon reperfusion. As a new type of cell death, ferroptosis provides new opportunities to reduce myocardial cell death. Ferroptosis is known to be more active during reperfusion than ischemia. However, the mechanisms regulating ferroptosis during ischemia and reperfusion remain largely unknown.

Methods: The contribution of ferroptosis in ischemic and reperfused myocardium were detected by administered of Fer-1, a ferroptosis inhibitor to C57BL/6 mice, followed by left anterior descending (LAD) ligation surgery. Ferroptosis was evaluated by measurement of cell viability, *ptgs2* mRNA level, iron production, malondialdehyde (MDA) and 4-hydroxynonenal (4-HNE) levels. H9C2 cells were exposed to hypoxia/reoxygenation to mimic in vivo I/R. We used LC-MS/MS to identify potential E3 ligases that interacted with frataxin in heart tissue. Cardiac-specific overexpression of frataxin in whole heart was achieved by intracardiac injection of frataxin, carried by adeno-associated virus serotype 9 (AAV9) containing cardiac troponin T (cTnT) promoter.

Results: We showed that regulators of iron metabolism, especially iron regulatory protein, were increased in the ischemic myocardium or hypoxia cardiomyocytes. In addition, we found that frataxin, which is involved in iron metabolism, is differentially expressed in the ischemic and reperfused myocardium and involved in the regulation of cardiomyocytes ferroptosis. Furthermore, we identified an E3 ligase, NHL repeat-containing 1 (NHLRC1), that mediates frataxin ubiquitination degradation. Cardiac-specific overexpression of frataxin ameliorated myocardial I/R injury through ferroptosis inhibition.

Conclusions: Through a multi-level study from molecule to animal model, these findings uncover the key role of frataxin in inhibiting cardiomyocyte ferroptosis and provide new strategies and perspectives for the treatment of myocardial I/R injury.

Keywords: myocardial ischemia/reperfusion injury, ischemia, ferroptosis, iron regulatory protein, NHLRC1

Abbreviations

AAV9, adeno-associated virus serotype 9; CCK-8, cell counting kit; cTnT, cardiac troponin T; ECG, electrocardiogram; EF, ejection fraction; FHC, ferritin heavy chain; FRDA, friedreich's ataxia; FS, fractional shortening; H/R, hypoxia/reoxygenation; HIF, hypoxia inducible factor; I/R, ischemia/reperfusion; IRP, iron regulatory protein; IVS, interventricular septum thickness; LAD, left anterior descending; LDH, lactate dehydrogenase; LVID, left ventricular internal diameter; LVPW, left ventricular posterior wall thickness; MDA, malondialdehyde; NHLRC1, NHL repeat-containing 1; NC, nontargeted control; NCOA4, nuclear receptor coactivator 4; SDH, succinate dehydrogenase; TFR, transferrin receptor; 4-HNE, 4-hydroxynonenal.

1. Introduction

Rapid revascularization through percutaneous coronary intervention has become the most effective therapy for the treatment of acute myocardial infarction. However, the restoration of blood flow inevitably leads to ischemia/reperfusion (I/R) injury that contributes to cardiac dysfunction, heart failure, arrhythmia and irreversible cardiomyocyte death [1]. Due to limited cardiac regenerative capacity, minimizing cardiomyocyte death is of particular importance to attenuate myocardial I/R injury.

Since the discovery of ferroptosis in 2012 by Stockwell et al. [2], this new mode of cell death has been extensively studied as a promising therapeutic strategy for the treatment of myocardial I/R injury. Recently, accumulating evidence has demonstrated that ferroptosis contributes to myocardial damage through I/R injury [3-6]. Notably, a recent study described the time frame for multiple forms of cell death during I/R injury, and ferroptosis is the predominant type of cardiomyocyte death after 24 h of reperfusion [7]. Moreover, the susceptibility to ferroptosis in the ischemia phase is increased through arachidonate-15-lipoxygenase-initiated redox reactions of polyunsaturated fatty acid phospholipids [8]. Ferroptosis is known to be more active during reperfusion than ischemia [9]. However, whether there are differences in the levels of ferroptosis in ischemia and reperfusion phases, as well as potential mechanisms, is still largely unknown. Therefore, a thorough understanding of the mechanisms involved in the regulation of cardiomyocyte ferroptosis during different phases of myocardial I/R injury will provide new strategies for the treatment.

Frataxin is a ubiquitously expressed mitochondrial protein implicated in the biogenesis of iron sulfur clusters to regulate the activity of iron sulfur proteins participating in various cellular processes such as mitochondrial oxidative respiration [10]. Deficiency in frataxin leads to the development of Friedreich's ataxia (FRDA), a neurodegenerative disease [11]. A retrospective study of FRDA patients showed the major cause of death was cardiac dysfunction (~59%) [12]. Nevertheless, the role of

frataxin in myocardial ischemia and subsequent I/R injury remains largely unknown.

In this study, we found that frataxin was induced in the ischemic myocardium and returned to normal during the reperfusion phase. In addition, frataxin-mediated iron metabolism inhibited ferroptosis in myocardial cells. We further explored the underlying cellular mechanisms and verified the cardioprotective effects of frataxin in vivo. Our findings provide insight into the pathogenic mechanisms that suppress ferroptosis in the myocardial ischemia and provide new strategies for therapy of I/R injury.

2. Material and methods

2.1. Mice

Male C57BL/6J mice (8–12 weeks old) were purchased from the Experimental Animal Center of the Fourth Military Medical University. Mice were housed at 25 °C, under a 12 h light/dark cycle with *ad libitum* access to water and diet. Animal protocols were approved by the Tab of Animal Experimental Ethical Inspection of Northwestern Polytechnical University (No. 202101123).

2.2. Reagents

RSL3 (S8155), ferrostatin-1 (S7243), MG132 (S2619) and Cell Counting Kit (CCK-8) were purchased from Selleck (Houston, TX). Antibodies to frataxin (ab219414), 4-hydroxynonenal (4-HNE, ab46545), ferritin heavy chain (FHC, ab183781), and transferrin receptor (TFR, ab269513) were obtained from Abcam (Cambridge, MA, USA). Antibodies against Flag (8146S), HA (3724S), and His (12698S) were from Cell Signaling Technology (Danvers, MA, USA). NFS1 (sc-365308), iron regulatory protein 1 (IRP1, sc-166022), and protein A/G PLUS-Agarose beads (sc-2003) were from Santa Cruz Biotechnology (Santa Cruz, CA, USA). Antibodies against NHL repeat-containing 1 (NHLRC1, A6669), IRP2 (A6382) and nuclear receptor coactivator 4 (NCOA4) were from ABclonal Technology (Wuhan, China). Antibody against GAPDH (CW0100M) and horseradish peroxidase-conjugated secondary antibodies were from CWBIO (Taizhou, China). 2,3,5-triphenyltetrazolium (TTC) was purchased from Sigma-Aldrich (St. Louis, MO, USA). Lactate dehydrogenase (LDH) detection kit was from Nanjing Jiancheng Bioengineering Institute (Nanjing, China). Malondialdehyde (MDA) assay kit, 4',6-diamidino-2-phenylindole (DAPI), and FITC/TRICT-labeled goat anti-rabbit/mouse IgG were purchased from Beyotime (Shanghai, China). Iron assay kit (ab83366) and aconitase assay kit (ab83459) were from Abcam (Cambridge, MA, USA). Lipofectamine 2000 was from Thermo Fisher Scientific (Waltham, MA, USA). Succinate dehydrogenase (SDH) activity assay kit (E-BC-K649-M) was purchased from Elabscience Biotechnology (Wuhan, China).

2.3. Establishment of ischemia and I/R injury mouse model

An ischemia mouse model was established by left anterior descending (LAD) coronary artery ligation surgery according to previous studies [13, 14]. In brief, male C57BL/6J mice were anaesthetized with 2% isoflurane and maintained at 37 °C with a heating pad; the trachea was then intubated to connect with a small animal ventilator to maintain respiration. Next, electrocardiogram (ECG) leads were connected. After opening the thoracic cavity, the LAD coronary artery was occluded using a 7-0 polypropylene sutures to cause myocardial ischemia for the indicated period of time, and ischemia was verified by an elevated ST segment in ECG. Success was marked by a lightening of color of the ventricular muscle distal to the ligature and marked elevation of the ST segment as seen on ECG. For the I/R injury group, the thread was loosened for reperfusion. At times indicated, the left ventricle or the whole heart was isolated for further experimentation. Sham-operated mice, with no ligation, were used as a control.

2.4. In vivo drug treatment

Male C57BL/6J mice were anaesthetized as indicated above. Mice were then administered Fer 1 (5 mg/kg, tail vein injection) or a solvent control. Five minutes later, LAD ligation was performed for 30 min and then reperfusion for 2 h.

2.5. Adeno-associated virus (AAV9) injection

Whole-heart overexpression of frataxin was achieved by intracardiac injection of AAV9 carrying mouse frataxin containing the cTNT promoter (AAV9-Fxn, 1.09×10^{14} vg/ml) or the corresponding control (AAV9-NC, 4.83×10^{13}vg/ml) (Vigene Biosciences, China) as we previously described [15]. After anesthetized using 2% isoflurane, mice were injected directly into the heart at three sites. 4 weeks post-injection, LAD ligation experiments were initiated.

2.6. Measurement of myocardial infarct size

Myocardial infarct size was measured as previously described [14]. After 4 h of reperfusion hearts were excised, intra-aortic infused with 2% TTC in phosphate solution, simultaneously the whole hearts were incubated in the TTC solution for 30 min at 37 °C. Heart tissue was then fixed in 4% paraformaldehyde for 24 h and cut into 1 mm slices. Sections were photographed and analyzed with ImageJ.

2.7. Echocardiography

Echocardiography was performed using a Vevo 3100LT (Fujifilm Visualsonics, Canada) in M-mode. Mice were anesthetized by isoflurane inhalation, the chest hair was shaved, and the animal was fixed to the detection board. The left ventricular long axis and short axis view were acquired. Interventricular septum thickness (IVS), left ventricular internal diameter (LVID), left ventricular posterior wall thickness (LVPW), ejection fraction (EF) and fractional shortening (FS) were measured.

2.8. Measurement of LDH activity

Serum was collected and analyzed with LDH detection kit per manufacturer's instructions. Briefly, samples were mixed with matrix buffer and coenzyme I, incubated for 15 min at 37 ℃, followed by the addition of 2-4-dinitrophenylhydrazine, and incubated for another 15 min at 37 ℃. Finally, 0.4 mol/L NaOH was added and incubation continued for 15 min at room temperature. Absorbance was measured at 450 nm, and LDH activity was represented as U/L.

2.9. MDA detection

Cardiac MDA levels were detected using MDA assay kit in accordance with the manufacturer's instructions [16].

2.10. Iron measurement

Iron levels were determined using an Iron Assay Kit using manufacturer's instruction. The product of ferrous iron (Fe^{2+}) with the iron probe has an absorbance at 593nm. The

iron level was normalized to the protein concentration.

2.11. Aconitase activity detection

Aconitase activity was measured using Aconitase Assay Kit (ab83459, Abcam). Fresh tissue samples were harvested, and cytosolic fractions isolated following manufacturer's instructions. Cysteine HCl and $(NH4)_2Fe(SO_4)_2$ was added to the samples to activate aconitase, the reaction mix from the kit was then added to samples and standards, these were incubated for 30 min, and absorbance was then measured at 450 nm.

2.12. SDH activity

The mitochondrial fractions from cardiac tissue samples were isolated, and SDH activity analyzed using SDH activity assay kit according to the manufacturer's instructions.

2.13. Cell culture

H9C2 cells, an embryonic rat myoblast cell line, and 293T cells, were purchased from ATCC and cultured in Dulbecco's modified Eagle's medium (Gibco) with 10% fetal bovine serum and 1% penicillin streptomycin mixture in 5% CO_2 at 37℃. For hypoxia/reoxygenation (H/R) experiments, H9C2 cells were cultured in 95% N_2 and 5% CO_2 for indicated time course, and reoxygenated in 95% air and 5% CO_2 as described previously [17].

2.14. Cell viability assay

Cell viability assay was performed using CCK-8 per manufacturer's instructions. H9C2 cells were seeded at 5×10^3 cells per well to a 96-well plate. After indicated treatment, 10 μL of CCK-8 was added to each well. After further incubation for 1 h at 37℃, absorbance at 450 nm was determined. Cell viability was represented as a percentage of the control group.

2.15. siRNA Transfection

H9C2 cells were transfected with nontargeted control (NC), frataxin, or NHLRC1 siRNA using Lipofectamine 2000 according to the manufacturer's instructions. The siRNA sequences used were: si-NHLRC1, 5'-CTCCAGTATGCAGCTGATT-3' and si-frataxin, 5'-CTGACTGAAGCTTTAAACA-3'.

2.16. Plasmid transfection

The Flag-frataxin and HA-NHLRC1 plasmids were made by inserting digested PCR products into a pCDNA3.1(+) vector. His-ubiquitin was a gift from Dr. Liu (Xi'an Jiao Tong University). 293T cells were transfected with plasmids using Lipofectamine 2000 according to the manufacturer's instructions.

2.17. Adenovirus delivery

H9C2 cells were infected with frataxin adenovirus (Ad-Frataxin, Vigene Biosciences, China) or a control for the virus vector. The adenovirus titer used in this study was 2.5 $\times 10^{11}$ PFU/ml, and the multiplicity of infection (MOI) was 200:1.

2.18. Histological and immunohistochemical analysis

Slides containing fixed heart tissue were processed for 4-HNE and frataxin expression as previously described [18]. Briefly, after antigen retrieval by incubating in antigen retrieval solution in a pressure cooker for 20 min at high temperature, the slides were pretreated with 3% hydrogen peroxide for 25 minutes in the dark. Then the slides were blocked with 5% bovine serum albumin for 30 min, and incubated with the primary antibodies to 4-HNE (1:200), frataxin (1:200) overnight, followed by incubation with secondary antibody (1:500) at room temperature for 1 h. Images were obtained on microscope using NIS Elements software. Masson's trichrome staining was used to assess fibrosis, and fibrosis was analyzed Image J.

2.19. Immunofluorescence

293T cells were transfected with plasmids for 48 h as described above. After fixation with 4% paraformaldehyde, the cells were blocked with 5% bovine serum albumin for 1 h and then incubated with antibody against HA and Flag at 4 ℃ overnight, followed by incubation with FITC/TRICT-labeled goat anti-rabbit IgG for 1 h at room temperature. Nuclei were stained with DAPI. All images were taken with a confocal laser scanning microscope (FV3000, Olypus).

2.20. Quantitative real-time PCR

Total RNA was isolated using Trizol reagent (Invitrogen, Carlsbad, CA). Quantitative PCR was performed using TB Green Premix Ex Taq (Takara) and a CFX96 Real-Time System (Bio-Rad). Gene expression was performed using the $2^{-\triangle\triangle Ct}$ method normalized to GAPDH. The PCR primers used were: ptgs2 (mouse), forward 5′-TGAGTACCGCAAACGCTTCT-3′ and reverse 5′-CAGCCATTTCCTTCTCTCCTG T-3′; GAPDH (mouse), forward 5’-ACCACAGTCCATGCCATCAC-3’ and reverse 5’-TCCACCACCCTGTTGCTGTA-3’; frataxin(rat), 5’-GCCATCCGCCACTCTCA TTT-3’ and 5’-CCTTCAGGGTGTAGGGCTTG-3’; NHLRC1 (rat), forward 5’-CGACTGCTCCCTCAAAGTGT-3’ and reverse 5’-CCCTTAGGGAAATCCGCTT- 3’ GAPDH (rat), forward 5’-ACAGCAACAGGGTGGTGGAC-3’ and reverse 5’-TTTGAGGGTGCAGCGAACTT-3’.

2.21. Immunoblots and immunoprecipitation

Proteins were isolated in RIPA buffer supplemented with protease inhibitors [19]. Protein concentrations were measured using the BCA kit per manufacturer’s instructions. Immunoblotting was performed with the appropriate antibodies followed by chemiluminescence detection. Immunoprecipitation was performed according to a protocol described previously [20]. Briefly, protein lysates were incubated with appropriate antibodies or IgG at 4 ℃ for 1 h, then with protein A/G PLUS-agarose

beads at 4 ℃ overnight. Immunoprecipitates were washed with RIPA buffer, then boiled for immunoblotting.

2.22. LC-MS/MS Analysis

SDS-PAGE was used to separate proteins after immunoprecipitation with frataxin antibody and protein A/G PLUS-agarose beads, the resulting gel bands at the expected sizes were excised and digested to extract peptides. Peptides were then subjected to tandem mass spectrometry (MS/MS) using Q ExactiveTM Plus coupled online to the UPLC. The resulting MS/MS data were processed using Proteome Discoverer 1.3.

2.23. Statistical Analysis

Data are given as the mean ± SEM. Comparisons were performed using student's t-test for two groups and one-way analysis of variances for more than two group with post hoc tests using GraphPad Prism 9.0 (GraphPad Software, San Diego, CA, USA). $P<0.05$ was considered statistically significant.

3. Results

3.1. Different degrees of ferroptosis during myocardial ischemia and reperfusion stages

Ferroptosis exists in both of the two major phases leading to myocardial injury, ischemia and reperfusion [7, 8]. To determine whether the contribution of ferroptosis varies by phase, C57BL/6 mice were administered a single dose of 5 mg/kg Fer-1, a ferroptosis inhibitor [21], followed by LAD ligation surgery for ischemia only or with induced I/R. Reperfusion decreased serum LDH levels induced with myocardial ischemia, and Fer-1 reduced LDH levels both in ischemic and reperfusion phases (Figure 1A). Indicators of ferroptosis [22] showed marked effects with reperfusion over the ischemic phase; cardiac *ptgs2* mRNA levels (Figure 1B), MDA levels (Figure 1C), and Fe^{2+} levels (Figure 1D) were all higher in the reperfusion phase. In addition, immunohistochemistry revealed a marked induction for 4-HNE in the reperfusion phase compared to the ischemic phase (Figure 1E). Taken together, these data suggest that the degree of ferroptosis differed during cardiac ischemia-reperfusion, where the degree of ferroptosis was more pronounced during reperfusion than ischemia.

3.2. IRP activity varies in the cardiac ischemia and reperfusion

Next, we measured the iron ion level in cytoplasm and mitochondria in both ischemia and reperfusion cardiac tissue. Interestingly, we found a significant accumulation of mitochondrial iron rather than cytoplasmic (Figure 2A-B). Given the importance of IRP activity in iron homeostasis [23], we explored IRP expression and activity in the cardiac ischemia and reperfusion further. As shown in Figure 2C-D, the protein levels of IRP1 and IRP2 did not differ between ischemia and reperfusion. Since IRP post-transcriptionally mediates FHC and TFR expression, we sought to assess FHC and TFR protein levels. C57BL/6 mice were subjected to LAD ligation surgery for different time periods (0, 15, 30, and 60 min). Results showed that protein expression of FHC increased while TFR protein levels decreased in a time dependent manner during ischemia (Figure 2E-G). While in the reperfusion phase, FHC protein expression

decreased in combination with the induction of TFR protein levels (Figure 2H-J). Using the in vitro H/R model to mimic in vivo I/R, H9C2 cells were exposed to hypoxia (oxygen below 1%) for the indicated time period (0, 3, 6, 12 h). Consistent with the in vivo results above, induced FHC expression and decreased TFR levels were time dependent with hypoxia exposure (Figure 2K-M), while reoxygenation abrogated the production of FHC as well as the inhibition of TFR induced by hypoxia (Figure 2M-P). NCOA4 acts as the cargo receptor mediating autophagic turnover of ferritin, termed ferritinophagy [24]. We further found that NCOA4 protein level decreased in the ischemia hearts and elevated in the reperfusion hearts (Figure S1A). Hypoxia exposure in H9C2 cells also decreased NCOA4 level in a time dependent manner (Figure S1B), in contrast, reoxygenation promoted the production of NCOA4 compared with hypoxia (Figure S1C). These data highlight the relevance of decreased IRP activity in cardiac reperfusion stage.

Considering that IRP1 also functions as a cytosolic aconitase in addition to regulating iron ion metabolism, we next tested aconitase activity with ischemia and reperfusion. The ischemic myocardium displayed increased cytoplasmic aconitase activity; however, in comparison, the reperfused myocardium revealed a marked reduction in cytoplasmic aconitase activity (Figure 2Q). Meanwhile, the altered activity of mitochondrial SDH, as an iron-sulfur protein, was consistent with aconitase activity with both ischemia and reperfusion (Figure 2R). These results illustrate the altered activity of Fe-S proteins.

3.3. Frataxin is upregulated in ischemic myocardium

To determine the upstream modulators regulating Fe-S protein activity, we investigated the expression of NFS1, an iron sulfur cluster biosynthetic enzyme, and frataxin, a key molecule in iron sulfur cluster biosynthesis. C57BL/6 mice were subjected to ischemia over the indicated time periods; western blot showed a significant increase of frataxin protein levels after 15 min, while NFS1 expression was not affected during ischemia (Figure 3A-B). Upon reperfusion, increased frataxin levels were attenuated, without

affecting NFS1 levels (Figure 3C-D). Moreover, H9C2 cells exposed to hypoxia displayed an increase in frataxin expression (Figure 3E-F), and reoxygenation exposure diminished the induction of frataxin compared to the hypoxia group (Figure 3G-H), consistent with ischemia/reperfusion data in vivo. These results suggest that frataxin was induced during the ischemic/hypoxia phase in vivo and in vitro; however, reperfusion/reoxidation reversed the induction back to normal levels.

3.4. Frataxin mediates RSL3-induced ferroptosis

To confirm the idea that frataxin regulates ferroptosis in cardiomyocytes, frataxin was suppressed or overexpressed in vitro. H9C2 cells were transfected with siRNA to knockdown frataxin expression. Three siRNA sequences targeting frataxin were utilized and mRNA levels and protein expression of frataxin were measured to evaluate knockout efficiency. As shown in Figure 4A-B, only siRNA2 worked, so it was used in subsequent experiments. H9C2 cells were first transfected with siRNA against frataxin for 48h and then exposed to cumulative doses of RSL3, a known inducer of ferroptosis [2], and Fer-1 was used as a positive control. CCK8 revealed that knockdown of frataxin markedly sensitized H9C2 cells to RSL3-induced ferroptosis (Figure 4C). To overexpress frataxin, H9C2 cells were infected with frataxin adenovirus of different MOI (Figure 4D). As expected, overexpression of frataxin inhibited the sensitivity of H9C2 cells to RSL3-induced ferroptosis (Figure 4E). Next, we measured TFR and FHC protein levels after transfected with siRNA to frataxin in H9C2 cells. It showed that knockdown of frataxin decreased FHC protein expression and induced TFR protein level (Figure 4F-G). These results illustrate the significant role of frataxin in ferroptosis sensitivity regulation, where loss of frataxin sensitized cells to ferroptosis.

3.5. E3 ligase NHLRC1 promotes frataxin ubiquitination

Studies have shown that frataxin can be degraded through ubiquitination, and given that the protein expression of frataxin changes over such a short period of time, we further explored whether frataxin ubiquitination leads to its differential expression during

ischemia and reperfusion and sought potential E3 ligases for its ubiquitination. In the presence of MG132 (a proteasome inhibitor) over different time courses, the level of frataxin ubiquitination rose, accompanied by increasing protein levels of frataxin (Figure S2). After frataxin was overexpressed in mouse heart by direct injection of AAV9-cTNT-Frataxin, separated and SDS-PAGE-isolated proteins were subjected to LC-MS/MS to identify potential E3 ligases that interacted with frataxin in heart samples. It showed that only one E3 ligase NHLRC1, combined with frataxin (Figure S3). We then verified the expression of NHLRC1 in both myocardial ischemia and reperfusion by immunoblotting and showed decreased NHLRC1 levels with ischemia compared with sham control mice. In contrast, NHLRC1 expression was induced with reperfusion as compared with ischemia (Figure 5A-B). Knockdown of NHLRC1 by siRNA transfection raised frataxin protein expression without affecting mRNA levels (Figure 5C-E). To determine whether frataxin is a substrate for NHLRC1, we examined the protein expression of frataxin in 293T cells with ectopic expression of frataxin alone or together with NHLRC1. We observed that NHLRC1 reduced the abundance of frataxin in a dose-dependent manner (Figure 5F). In addition, 293T cells were transfected with both HA-tagged NHLRC1 and Flag-tagged frataxin, and immunofluorescence showed co-localization of exogenous NHLRC1 and frataxin (Figure 5G). In accordance with this, immunoprecipitation of Flag followed by immunoblotting showed that NHLRC1 bound to frataxin (Figure 5H). As K48 is the main lysine in ubiquitin that guides proteasomal degradation, a mutation of the K48 lysine to arginine (K48R) was generated to determine whether K48R affected frataxin ubiquitination. We demonstrated that K48R prevented ubiquitination of frataxin compared with wild type ubiquitin (Figure 5I), suggesting that NHLRC1 promoted K48-linked polyubiquitination of frataxin. K147 in frataxin is a known ubiquitination target [25], so we next generated frataxin mutants by replacing that lysine with arginine (K147R). The K147R mutation also decreased interaction between NHLRC1 and frataxin, as well as the level of frataxin ubiquitination (Figures 5J). Taken together, these data illustrate that the E3 ligase NHLRC1 interacted with frataxin at its K147 site to mediate the

ubiquitination and subsequent degradation of frataxin.

3.6. Knockdown of NHLRC1 decreases RSL3-induced ferroptosis in cardiomyocytes

To investigate the role of NHLRC1 in ferroptosis, H9C2 cells were transfected with NHLRC1 siRNA for 36 h, then co-incubated with RSL3 for 24 h. We found that NHLRC1 siRNA prevented RSL3-induced decrease in cell viability compared with NC (Figure 6A). We then measured *ptgs2* mRNA, MDA, and iron levels. As expected, *ptgs2* mRNA (Figure 6B), MDA (Figure 6C), and iron (Figure 6D) levels were all remarkably decreased after NHLRC1 knockdown. These results indicate that NHLRC1 knockdown could decrease RSL3-induced ferroptosis in cardiomyocytes.

3.7. Cardiac-specific frataxin overexpression protects against myocardial I/R injury

To verify the essential role of frataxin in susceptibility to myocardial I/R injury, a cardiac-specific overexpression of frataxin model was established by direct intracardiac injection of frataxin carried by AAV9 containing a cTNT promoter. The expression of frataxin was detected after 4 weeks. Immunoblotting revealed that frataxin was overexpressed only in myocardial tissue but not in muscle or liver tissues (Figure 7A-B), and consistently, immunohistochemistry showed overexpression of frataxin in heart tissue (Figure 7C). These results proved that cardiac-specific overexpression of frataxin model was successfully established. The mice were then subjected to I/R injury. Frataxin overexpression provided protective effects against I/R injury, represented by reduced serum levels of LDH (Figure 7D), decreased infract size (Figure 7E-F), and improved cardiac function (Figure 7G-I). Noticeably, myocardial infarct size was significantly decreased in frataxin-overexpressed hearts (Figure 7E-F), and echocardiographic results showed improved cardiac function with significant increases of EF and FS compared to I/R mice (Figure 7G-I). In addition, Masson's trichrome staining indicated reduced fibrosis in frataxin-overexpressed hearts compared with

AAV-NC group after I/R (Figure S4A-B). Taken together, these data provide evidence that cardiac-specific frataxin overexpression decreased susceptibility to myocardial I/R injury.

3.8. Frataxin overexpression inhibits myocardial ferroptosis in vivo

We also measured ferroptosis levels in cardiac-specific frataxin overexpression mice followed by I/R injury. With I/R, *ptgs2* mRNA levels were decreased in frataxin-overexpressed mice compared with AAV9 control group (Figure 8A). MDA levels (Figure 8B) and Fe^{2+} levels (Figure 8C) were also reduced in frataxin-overexpressed tissue with I/R injury as compared with the I/R only group. Immunohistochemistry showed increased 4-HNE levels in the AAV9 control group with I/R injury, which was attenuated in frataxin-overexpressed mice (Figure 8D). We also measured aconitase activity and found that aconitase activity was increased in frataxin-overexpressed mice, but in the I/R injury only group aconitase activity was decreased, whereas frataxin overexpression with I/R injury attenuated the increase of aconitase activity (Figure 8E) back to normal levels. Furthermore, frataxin overexpression increased FHC and frataxin levels myocardial I/R, but decreased TFR levels at the same time (Figure 8F-I).

Taken together, we found a novel E3 ligase NHLRC1 that mediated the ubiquitination of frataxin in myocardial I/R. Cardiac-specific frataxin overexpression in mice prevented ferroptosis to improve cardiac function through regulation of iron metabolism. Therefore, targeting frataxin provides a potential strategy for I/R therapy.

4. Discussion

In this study, we show that the upregulation of frataxin in the ischemic myocardium is a suppressor of ferroptosis. We also show that cardiac-specific frataxin overexpression ameliorates I/R injury through ferroptosis inhibition (Graphical Abstract). At the cellular level, our studies provide a mechanism for the anti-ferroptosis effect exerted by frataxin in ischemia, where decreased NHLRC1 E3 ligase expression reduced frataxin ubiquitination degradation to inhibit ferroptosis through an IRP1-related pathway. At the disease level, we demonstrated that frataxin inhibited cardiomyocyte ferroptosis to ameliorate myocardial I/R injury in vivo and in vitro. Our study elucidated the mechanism underlying myocardial I/R injury, providing potential therapeutic targets for I/R injury treatment.

Studies in acute myocardial infarction animal models indicate that lethal reperfusion injury accounts for 50% of the final size of myocardial infarction [26]. In most cases, pharmacological inhibitors of cell death signaling reduce cardiomyocyte death and infarct size only in the reperfused myocardium and less in cardiomyocytes subjected to permanent ischemia [27]. The body's own cellular repair processes may begin soon after the ischemic phase to mitigate ischemic tissue damage, an essential cardioprotective strategy for the treatment of myocardial infarction and I/R injury. A classic example of this is AMPK, an essential sensor to modulate metabolism homeostasis during myocardial ischemia. Here in our study, we found that frataxin was induced in ischemic hearts but had decreased expression in the reperfused myocardium, suggesting decreased cardioprotective effects for frataxin in I/R injury. Overexpression of frataxin was able to reduce myocardial infarct size and improve cardiac function. This novel discovery provides a potential therapeutic target for I/R injury.

IRPs are key regulators of iron homeostasis [28]. IRP1 and IRP2 share high sequence homology [29], maintain iron balance through post transcriptional regulation of IRP/IRE regulatory system. IRP1 and IRP2 recognize untranslated mRNA regions for

TFR and ferritin H, respectively, to upregulate TFR and reduce ferritin regulation and iron acquisition and storage. Notably, IRP1 is a bifunctional protein: when iron and iron sulfur clusters are abundant, IRP1 contains a [4Fe-4S] cluster and functions as a cytosolic aconitase to participate in the tricarboxylic acid cycle; but with iron deficiency or when Fe-S clusters are absent, IRP1 binds IREs with high affinity to regulate iron homeostasis [30]. This IRP1-dependent mechanism sustains mitochondrial iron demand in liver-specific *Fxn* deletion mice [31]. Although sharing high sequence homology to IRP1, IPR2 lacks aconitase activity [32]. IRP2 also does not contain an Fe-S cluster and is regulated by iron-regulated ubiquitin ligase FBXL5-mediated ubiquitination and degradation [33]. Moreover, IRP2 is stabilized under hypoxic conditions in cell lines with established IRP2 expression [34, 35]. In our study, we found that activation of IRP in the myocardial ischemia was characterized by elevated TFR and reduced FHC (Figure 2). Subsequent experiments in vivo and in vitro showed that frataxin, a key molecule for iron sulfur cluster synthesis, but not NFS1, a key enzyme in iron-sulfur cluster biosynthesis, plays a role in regulating IRP1 activity, although NFS1 has been reported to protect tumor cells from ferroptosis [36]. However, several reports suggested that IRP2, not IRP1, dominates the post-transcriptional regulation of iron metabolism in vivo [29, 37, 38]. Possible explanations for this discrepancy include: 1) The expression of IRP1 and IRP2 varies in different tissues and cell types, and their respective roles are not identical; 2) Previous studies focused on elucidating the role of IRP1/2 at the basal level in a knockdown model, while the roles of IRP1/2 in pathological situations are more complicated; or 3) Previous studies only elucidated the role of IRP2 with oxygen concentrations at 3%-6%, and the dynamic alteration of IRP activity in different cell types or tissues at different oxygen levels needs to be further illustrated. More work is needed to untangle the discrepancies.

FRDA, a progressive neurodegenerative disease caused by insufficient expression of frataxin, is characterized by altered iron metabolism with mitochondrial iron loading [39]. It is interesting that in muscle of creatine kinase-conditional frataxin knockout

mice, reduced iron-sulfur cluster synthesis with frataxin deficiency led to further compensatory increases in iron transport to mitochondria, and chelation therapy ameliorated cardiac hypertrophy in mutated-frataxin mice [40]. Surprisingly, several studies have shown that high levels of frataxin led to mitochondrial and cardiac toxicity in mouse models [41, 42]. However, detrimental effects from the carrier delivery pathway or dosage levels cannot be excluded, and frataxin may have reached very high levels in the heart, cerebellum, or off target organs such as the liver. Using the chicken β-actin promoter for AAV9-based frataxin overexpression showed that toxic overexpression of frataxin can be achieved in mouse livers to trigger liver regeneration [41]. Here in our study, AAV9-frataxin containing the cTnT promoter achieved cardiac-specific expression of frataxin, minimizing off-target effects.

The *Fxn* gene encodes for a precursor form of frataxin in the cytosol, which contains an N-terminal mitochondrial localization signal. The precursor form of frataxin undergoes two-step proteolytic processing before importation into mitochondria, which first generate an intermediate form, and then produce the mature, functional form of frataxin [43, 44]. Frataxin maturation is evolutionarily highly conserved. Frataxin undergoes both transcriptional and posttranslational modifications. Frataxin is transcriptionally regulated by hypoxia inducible factor (HIF) 1α and HIF-2α [45, 46]. Src kinase phosphorylates frataxin on residue Y118 and promotes frataxin ubiquitination [47]. Before its mitochondrial import, frataxin precursor is degraded by the ubiquitin–proteasome system with K147 as the main ubiquitination target [25]. Recently, Benini et al. found that RNF126 specifically mediated frataxin ubiquitination and targeted it for degradation both in vitro and in cells derived from FRDA patients [48]. In this study, given the rapidly altered frataxin levels with ischemia and reperfusion (less than 1 h), a ubiquitination-related degradation mechanism for frataxin was investigated.

NHLRC1 (EPM2B) encodes the E3 ubiquitin ligase malin expression, and its mutations

causes Lafora disease through laforin accumulation and glycogen metabolism disorder [49]. Except being widely expressed in the nervous system, NHLRC1 is also expressed in left ventricular tissue [50]. We identified NHLRC1 as a new E3 ligase that mediates frataxin ubiquitination in this study. And one of the limitations is the mechanism that alters the expression of NHLRC1 in ischemic and reperfused hearts. MicroRNAs, oxygen content, or metabolites under ischemia may act as upstream signals to rapidly regulate the expression of NHLRC1.

Taken together, our results illustrate the critical role of frataxin in regulating ischemic versus reperfusion sensitivity to ferroptosis through direct ubiquitin degradation of frataxin by the E3 ligase NHLRC1. This suggests that targeting frataxin may be potential therapeutic strategy for the treatment of I/R injury.

Funding

This work was supported by the National Natural Science Foundation of China (No.82100312, 82070261, 82170251), National Key Research and Development Program of China (No.2021YFA1100501), the China Postdoctoral Science Foundation (No.2021M692640), the Youth Innovation Team of Shaanxi Universities, and the Innovation Foundation for Doctor Dissertation of Northwestern Polytechnical University (CX2022068).

Author contributions

Zihui Zhang designed of the study, performed the experiments and drafted the manuscript. Wenhua Jiang performed the animal experiments and analyzed the data. Chan Zhang and Yue Yin participated in part of the experiments. Nan Mu and Yishi Wang edited the manuscript. Lu Yu and Heng Ma designed the study, revised the manuscript and provided overall supervision for the study. The final version to be

submitted was approved by all authors.

Declaration of competing interest

The authors have declared that no competing interest exists.

References

1. J. Zhang, D. Liu, M. Zhang, and Y. Zhang. Programmed necrosis in cardiomyocytes: mitochondria, death receptors and beyond. Br J Pharmacol, 176 (2019), pp.4319-4339, 10.1111/bph.14363.

2. S.J. Dixon, K.M. Lemberg, M.R. Lamprecht, R. Skouta, E.M. Zaitsev, C.E. Gleason, et al. Ferroptosis: an iron-dependent form of nonapoptotic cell death. Cell, 149 (2012), pp.1060-1072, 10.1016/j.cell.2012.03.042.

3. X. Fang, H. Wang, D. Han, E. Xie, X. Yang, J. Wei, et al. Ferroptosis as a target for protection against cardiomyopathy. Proc Natl Acad Sci U S A, 116 (2019), pp.2672-2680, 10.1073/pnas.1821022116.

4. L.J. Tang, Y.J. Zhou, X.M. Xiong, N.S. Li, J.J. Zhang, X.J. Luo, et al. Ubiquitin-specific protease 7 promotes ferroptosis via activation of the p53/TfR1 pathway in the rat hearts after ischemia/reperfusion. Free Radic Biol Med, 162 (2021), pp.339-352, 10.1016/j.freeradbiomed.2020.10.307.

5. X. Fang, Z. Cai, H. Wang, D. Han, Q. Cheng, P. Zhang, et al. Loss of Cardiac Ferritin H Facilitates Cardiomyopathy via Slc7a11-Mediated Ferroptosis. Circ Res, 127 (2020), pp.486-501, 10.1161/circresaha.120.316509.

6. X. Fang, H. Ardehali, J. Min, and F. Wang. The molecular and metabolic landscape of iron and ferroptosis in cardiovascular disease. Nat Rev Cardiol, 20 (2023), pp.7-23, 10.1038/s41569-022-00735-4.

7. W. Cai, L. Liu, X. Shi, Y. Liu, J. Wang, X. Fang, et al. Alox15/15-HpETE Aggravates Myocardial Ischemia-Reperfusion Injury by Promoting Cardiomyocyte Ferroptosis. Circulation, (2023),10.1161/circulationaha.122.060257.

8. X.H. Ma, J.H. Liu, C.Y. Liu, W.Y. Sun, W.J. Duan, G. Wang, et al. ALOX15-launched PUFA-phospholipids peroxidation increases the susceptibility of ferroptosis in ischemia-induced myocardial damage. Signal Transduct Target Ther, 7 (2022), pp.288, 10.1038/s41392-022-01090-z.

9. J. Lillo-Moya, C. Rojas-Solé, D. Muñoz-Salamanca, E. Panieri, L. Saso, and R. Rodrigo. Targeting Ferroptosis against Ischemia/Reperfusion Cardiac Injury. Antioxidants (Basel), 10 (2021),10.3390/antiox10050667.

10. R. Lill and S.A. Freibert. Mechanisms of Mitochondrial Iron-Sulfur Protein Biogenesis. Annu Rev Biochem, 89 (2020), pp.471-499, 10.1146/annurev-biochem-013118-111540.

11. A.E. Harding. Friedreich's ataxia: a clinical and genetic study of 90 families with an analysis of early diagnostic criteria and intrafamilial clustering of clinical features. Brain, 104 (1981), pp.589-620, 10.1093/brain/104.3.589.

12. A.Y. Tsou, E.K. Paulsen, S.J. Lagedrost, S.L. Perlman, K.D. Mathews, G.R. Wilmot, et al. Mortality in Friedreich ataxia. J Neurol Sci, 307 (2011), pp.46-49, 10.1016/j.jns.2011.05.023.

13. C. Li, N. Mu, C. Gu, M. Liu, Z. Yang, Y. Yin, et al. Metformin mediates cardioprotection against aging-induced ischemic necroptosis. Aging Cell, 19 (2020), pp.e13096, 10.1111/acel.13096.

14. C. Li, W. Sun, C. Gu, Z. Yang, N. Quan, J. Yang, et al. Targeting ALDH2 for Therapeutic Interventions in Chronic Pain-Related Myocardial Ischemic Susceptibility. Theranostics, 8 (2018), pp.1027-1041, 10.7150/thno.22414.

15. F. Zhang, K. Wang, S. Zhang, J. Li, R. Fan, X. Chen, et al. Accelerated FASTK mRNA degradation induced by oxidative stress is responsible for the destroyed myocardial mitochondrial gene expression and respiratory function in alcoholic cardiomyopathy. Redox Biol, 38 (2021), pp.101778, 10.1016/j.redox.2020.101778.

16. N. Li, X. Yi, Y. He, B. Huo, Y. Chen, Z. Zhang, et al. Targeting Ferroptosis as a Novel Approach to Alleviate Aortic Dissection. Int J Biol Sci, 18 (2022), pp.4118-4134, 10.7150/ijbs.72528.

17. T. Li, Y. Yin, N. Mu, Y. Wang, M. Liu, M. Chen, et al. Metformin-Enhanced Cardiac AMP-Activated Protein Kinase/Atrogin-1 Pathways Inhibit Charged Multivesicular Body Protein 2B Accumulation in Ischemia-Reperfusion Injury. Front Cell Dev Biol, 8 (2020), pp.621509, 10.3389/fcell.2020.621509.

18. Y. Chen, X. Yi, B. Huo, Y. He, X. Guo, Z. Zhang, et al. BRD4770 functions as a novel ferroptosis inhibitor to protect against aortic dissection. Pharmacol Res, 177 (2022), pp.106122, 10.1016/j.phrs.2022.106122.

19. Z. Zhang, X. Xie, Q. Yao, J. Liu, Y. Tian, C. Yang, et al. PPARδ agonist prevents endothelial dysfunction via induction of dihydrofolate reductase gene and activation of

tetrahydrobiopterin salvage pathway. Br J Pharmacol, 176 (2019), pp.2945-2961, 10.1111/bph.14745.

20. J. Liu, Q. Yao, L. Xiao, F. Li, W. Ma, Z. Zhang, et al. APC/Cdh1 targets PECAM-1 for ubiquitination and degradation in endothelial cells. J Cell Physiol, 235 (2020), pp.2521-2531, 10.1002/jcp.29156.

21. X. Wei, X. Yi, X.H. Zhu, and D.S. Jiang. Posttranslational Modifications in Ferroptosis. Oxid Med Cell Longev, 2020 (2020), pp.8832043, 10.1155/2020/8832043.

22. Y. Chen, Z.M. Fang, X. Yi, X. Wei, and D.S. Jiang. The interaction between ferroptosis and inflammatory signaling pathways. Cell Death Dis, 14 (2023), pp.205, 10.1038/s41419-023-05716-0.

23. N. Wilkinson and K. Pantopoulos. The IRP/IRE system in vivo: insights from mouse models. Front Pharmacol, 5 (2014), pp.176, 10.3389/fphar.2014.00176.

24. J.D. Mancias, X. Wang, S.P. Gygi, J.W. Harper, and A.C. Kimmelman. Quantitative proteomics identifies NCOA4 as the cargo receptor mediating ferritinophagy. Nature, 509 (2014), pp.105-109, 10.1038/nature13148.

25. A. Rufini, S. Fortuni, G. Arcuri, I. Condò, D. Serio, O. Incani, et al. Preventing the ubiquitin-proteasome-dependent degradation of frataxin, the protein defective in Friedreich's ataxia. Hum Mol Genet, 20 (2011), pp.1253-1261, 10.1093/hmg/ddq566.

26. D.M. Yellon and D.J. Hausenloy. Myocardial reperfusion injury. N Engl J Med, 357 (2007), pp.1121-1135, 10.1056/NEJMra071667.

27. D.P. Del Re, D. Amgalan, A. Linkermann, Q. Liu, and R.N. Kitsis. Fundamental Mechanisms of Regulated Cell Death and Implications for Heart Disease. Physiological

reviews, 99 (2019), pp.1765-1817, 10.1152/physrev.00022.2018.

28. Y. Chen, Y. He, X. Wei, and D.S. Jiang. Targeting regulated cell death in aortic aneurysm and dissection therapy. Pharmacol Res, 176 (2022), pp.106048, 10.1016/j.phrs.2021.106048.

29. E.G. Meyron-Holtz, M.C. Ghosh, K. Iwai, T. LaVaute, X. Brazzolotto, U.V. Berger, et al. Genetic ablations of iron regulatory proteins 1 and 2 reveal why iron regulatory protein 2 dominates iron homeostasis. Embo j, 23 (2004), pp.386-395, 10.1038/sj.emboj.7600041.

30. W.E. Walden, A.I. Selezneva, J. Dupuy, A. Volbeda, J.C. Fontecilla-Camps, E.C. Theil, et al. Structure of dual function iron regulatory protein 1 complexed with ferritin IRE-RNA. Science, 314 (2006), pp.1903-1908, 10.1126/science.1133116.

31. A. Martelli, S. Schmucker, L. Reutenauer, J.R.R. Mathieu, C. Peyssonnaux, Z. Karim, et al. Iron regulatory protein 1 sustains mitochondrial iron loading and function in frataxin deficiency. Cell Metab, 21 (2015), pp.311-323, 10.1016/j.cmet.2015.01.010.

32. B. Guo, Y. Yu, and E.A. Leibold. Iron regulates cytoplasmic levels of a novel iron-responsive element-binding protein without aconitase activity. J Biol Chem, 269 (1994), pp.24252-24260.

33. A.A. Salahudeen, J.W. Thompson, J.C. Ruiz, H.W. Ma, L.N. Kinch, Q. Li, et al. An E3 ligase possessing an iron-responsive hemerythrin domain is a regulator of iron homeostasis. Science, 326 (2009), pp.722-726, 10.1126/science.1176326.

34. E.S. Hanson, M.L. Rawlins, and E.A. Leibold. Oxygen and iron regulation of iron regulatory protein 2. J Biol Chem, 278 (2003), pp.40337-40342,

10.1074/jbc.M302798200.

35. E. Bourdon, D.K. Kang, M.C. Ghosh, S.K. Drake, J. Wey, R.L. Levine, et al. The role of endogenous heme synthesis and degradation domain cysteines in cellular iron-dependent degradation of IRP2. Blood Cells Mol Dis, 31 (2003), pp.247-255, 10.1016/s1079-9796(03)00161-x.

36. S.W. Alvarez, V.O. Sviderskiy, E.M. Terzi, T. Papagiannakopoulos, A.L. Moreira, S. Adams, et al. NFS1 undergoes positive selection in lung tumours and protects cells from ferroptosis. Nature, 551 (2017), pp.639-643, 10.1038/nature24637.

37. E.G. Meyron-Holtz, M.C. Ghosh, and T.A. Rouault. Mammalian tissue oxygen levels modulate iron-regulatory protein activities in vivo. Science, 306 (2004), pp.2087-2090, 10.1126/science.1103786.

38. M.W. Hentze, M.U. Muckenthaler, B. Galy, and C. Camaschella. Two to tango: regulation of Mammalian iron metabolism. Cell, 142 (2010), pp.24-38, 10.1016/j.cell.2010.06.028.

39. M. Whitnall, Y. Suryo Rahmanto, M.L. Huang, F. Saletta, H.C. Lok, L. Gutiérrez, et al. Identification of nonferritin mitochondrial iron deposits in a mouse model of Friedreich ataxia. Proc Natl Acad Sci, 109 (2012), pp.20590-20595, 10.1073/pnas.1215349109.

40. M. Whitnall, Y. Suryo Rahmanto, R. Sutak, X. Xu, E.M. Becker, M.R. Mikhael, et al. The MCK mouse heart model of Friedreich's ataxia: Alterations in iron-regulated proteins and cardiac hypertrophy are limited by iron chelation. Proc Natl Acad Sci U S A, 105 (2008), pp.9757-9762, 10.1073/pnas.0804261105.

41. C. Huichalaf, T.L. Perfitt, A. Kuperman, R. Gooch, R.C. Kovi, K.A. Brenneman, et al. In vivo overexpression of frataxin causes toxicity mediated by iron-sulfur cluster deficiency. Mol Ther Methods Clin Dev, 24 (2022), pp.367-378, 10.1016/j.omtm.2022.02.002.

42. B. Belbellaa, L. Reutenauer, N. Messaddeq, L. Monassier, and H. Puccio. High Levels of Frataxin Overexpression Lead to Mitochondrial and Cardiac Toxicity in Mouse Models. Mol Ther Methods Clin Dev, 19 (2020), pp.120-138, 10.1016/j.omtm.2020.08.018.

43. K.Z. Bencze, K.C. Kondapalli, J.D. Cook, S. McMahon, C. Millán-Pacheco, N. Pastor, et al. The structure and function of frataxin. Crit Rev Biochem Mol Biol, 41 (2006), pp.269-291, 10.1080/10409230600846058.

44. I. Condò, N. Ventura, F. Malisan, A. Rufini, B. Tomassini, and R. Testi. In vivo maturation of human frataxin. Hum Mol Genet, 16 (2007), pp.1534-1540, 10.1093/hmg/ddm102.

45. G. Nanayakkara, A. Alasmari, S. Mouli, H. Eldoumani, J. Quindry, G. McGinnis, et al. Cardioprotective HIF-1α-frataxin signaling against ischemia-reperfusion injury. American journal of physiology. Heart and circulatory physiology, 309 (2015), pp.H867-879, 10.1152/ajpheart.00875.2014.

46. Y. Oktay, E. Dioum, S. Matsuzaki, K. Ding, L.J. Yan, R.G. Haller, et al. Hypoxia-inducible factor 2alpha regulates expression of the mitochondrial aconitase chaperone protein frataxin. J Biol Chem, 282 (2007), pp.11750-11756, 10.1074/jbc.M611133200.

47. F. Cherubini, D. Serio, I. Guccini, S. Fortuni, G. Arcuri, I. Condò, et al. Src

inhibitors modulate frataxin protein levels. Hum Mol Genet, 24 (2015), pp.4296-4305, 10.1093/hmg/ddv162.

48. M. Benini, S. Fortuni, I. Condò, G. Alfedi, F. Malisan, N. Toschi, et al. E3 Ligase RNF126 Directly Ubiquitinates Frataxin, Promoting Its Degradation: Identification of a Potential Therapeutic Target for Friedreich Ataxia. Cell Rep, 18 (2017), pp.2007-2017, 10.1016/j.celrep.2017.01.079.

49. M.S. Gentry, C.A. Worby, and J.E. Dixon. Insights into Lafora disease: malin is an E3 ubiquitin ligase that ubiquitinates and promotes the degradation of laforin. Proc Natl Acad Sci U S A, 102 (2005), pp.8501-8506, 10.1073/pnas.0503285102.

50. M.E. Adriaens, E.M. Lodder, A. Moreno-Moral, J. Šilhavý, M. Heinig, C. Glinge, et al. Systems Genetics Approaches in Rat Identify Novel Genes and Gene Networks Associated With Cardiac Conduction. J Am Heart Assoc, 7 (2018), pp.e009243, 10.1161/jaha.118.009243.

Figure Legends

Figure 1. Ferroptosis levels in heart tissue from mice with induced ischemia or I/R. Serum LDH levels (A); cardiac *ptgs2* mRNA (B), MDA (C), iron (D) levels; and 4-HNE levels (E) were measured in mice subjected to sham, 30 min of ischemia (I), Fer-1 (5mg/kg) for 5 min followed by ischemia for 30 min (Fer-1+I), 30 min of ischemia followed by 2 h of reperfusion (I/R), or Fer-1 (5mg/kg) for 5 min followed by I/R (Fer-1+I/R), scale bar=20 μm. Data are shown as mean ± SEM, n=5. *$P < 0.05$, **$P < 0.01$ vs. sham; $^{\#}P < 0.05$, $^{\#\#}P < 0.01$ vs. I; $^{\&}P < 0.05$, $^{\&\&}P < 0.01$ vs. I; $^{\ddagger}P < 0.05$, $^{\ddagger\ddagger}P < 0.01$ vs. I/R.

Figure 2. Altered IRP activity in myocardial ischemia and reperfusion. Cytoplasmic (A) and mitochondrial (B) iron in sham, ischemic, and I/R hearts. (C) Western blot analysis of IRP1/2 in sham, ischemic, and I/R hearts. (D) Quantification of IRP1 and IRP2 levels normalized to GAPDH. (E) FHC and TFR protein levels were detected in ischemia over the indicated time period (0, 15, 30, 60 min). (H) FHC and TFR protein levels were measured in sham, ischemic, and I/R hearts. (K) FHC and TFR protein levels were detected in H9C2 cells exposed to hypoxia (with oxygen below 1%) over the indicated time period (0, 3, 6, 12 h). (N) H9C2 cells were exposed to normal, hypoxia, or hypoxia/reoxygenation (1, 3, 6 h) conditions and FHC and TFR protein expression was measured. (F), (G), (I), (J), (L), (M), (O) and (P) were quantification of FHC and TFR levels were normalized to GAPDH. Aconitase activity (Q) and SDH activity (R) were measured in sham, ischemic, and I/R hearts. Data are shown as mean ± SEM, n=3-5. *$P < 0.05$, **$P < 0.01$ vs. sham or control; $^{\#}P < 0.05$, $^{\#\#}P < 0.01$ vs. I or H; $^{\&}P < 0.05$ vs. R1.

Figure 3. Frataxin was upregulated in myocardial ischemia and returned to normal in myocardial I/R. (A) Frataxin and NFS1 protein levels were detected with ischemia only over the indicated time period (0, 15, 30, 60 min). (C) Frataxin and NFS1 protein levels were measured in sham, ischemic, and I/R hearts. (E) Frataxin and NFS1

protein levels were detected in H9C2 cells exposed to hypoxia (with oxygen below 1%) over the indicated time period (0, 3, 6, 12 h). (G) H9C2 cells were exposed in normal, hypoxia, or hypoxia/reoxygenation (1, 3, 6 h) conditions, and frataxin and NFS1 protein expression was measured. In (B), (D), (F), and (H), quantification of frataxin and NFS1 levels were normalized to GAPDH. Data are shown as mean ± SEM, n=3-5. $^{*}P < 0.05$, $^{**}P < 0.01$ vs. sham or control; $^{\#}P < 0.05$, $^{\#\#}P < 0.01$ vs. I or H.

Figure 4. Frataxin regulated RSL3-induced ferroptosis in vitro. H9C2 cells were transfected with three different frataxin siRNAs; the mRNA levels (A) and protein expression (B) of frataxin were detected. (C) H9C2 cells were transfected with frataxin siRNA for 36 h or pretreated with Fer-1 (1 μM) for 2 h then exposed to cumulative doses of RSL3, followed by CCK8 assay. (D) H9C2 cells were infected with frataxin adenovirus with different MOI; frataxin protein expression was detected. (E) H9C2 cells were infected with frataxin adenovirus (MOI=200) for 36 h or pretreated with Fer-1 (1 μM) for 2 h, and then stimulated with cumulative doses of RSL3, cell viability was assayed by CCK8 assay. (F) H9C2 cells were transfected with frataxin siRNA for 36 h, frataxin, FHC and TFR protein levels were measured. (G) Quantification of frataxin, FHC and TFR levels. Data are shown as mean ± SEM, n=3-5. $^{*}P < 0.05$, $^{**}P < 0.01$ vs. NC or GFP.

Figure 5. NHLRC1 directed frataxin for ubiquitination degradation. (A) Western blot analysis of NHLRC1 in sham, ischemic, and I/R heart tissue. (B) Quantification of NHLRC1 levels normalized to GAPDH. H9C2 cells were transfected with NHLRC1 siRNA, and mRNA levels of *nhlrc1* (C) and *fxn* (D) and protein expression of NHLRC1 and frataxin (E) were measured. (F) 293T cells were transfected with Flag-tagged frataxin, and in the presence or absence of accumulated HA-tagged NHLRC1 for 48 h, Flag and HA levels were analyzed by western blot. (G) 293T cells were transfected with Flag-tagged frataxin, and in the presence or absence of HA-tagged NHLRC1 for 48 h, Flag and HA expression were analyzed by confocal microscopy, scale bar=20 μm. (H)

Immunoblotting analysis of whole cell lysates and immunoprecipitation derived from 293T cells transfected with Flag-tagged frataxin or HA-tagged NHLRC1. (I) 293T cells, transfected with Flag-tagged frataxin, HA-tagged NHLRC1, or the indicated His-Ub plasmids, immunoblot analysis of whole cell lysates and immunoprecipitation to detect ubiquitination of frataxin. (J) 293T cells, transfected with Flag-tagged frataxin, Flag-tagged frataxin (K147R), HA-tagged NHLRC1, or His-Ub, immunoblot analysis of whole cell lysates and immunoprecipitation to detect ubiquitination of frataxin, as well as the interaction of frataxin and NHLRC1. Data are shown as mean ± SEM, n=3-5. *$P < 0.05$, **$P < 0.01$ vs. sham or NC; $^{\#}P < 0.05$, $^{\#\#}P < 0.01$ vs. I.

Figure 6. Knockdown of NHLRC1 inhibited ferroptosis. H9C2 cells were transfected with NHLRC1 siRNA for 36 h, followed by coincubation with RSL3 for another 24 h; cell viability was assayed by CCK8 assay (A), and cardiac *ptgs2* mRNA (B), MDA (C), and iron (D) levels were detected. Data are shown as mean ± SEM, n=3-5. *$P < 0.05$, **$P < 0.01$ vs. control; $^{\#}P < 0.05$, $^{\#\#}P < 0.01$ vs. siNHLRC1.

Figure 7. Frataxin overexpression protected against I/R injury. (A) C57BL/6 mice were given intracardiac injections of AAV9-frataxin containing the cTNT promoter or AAV9-NC. After 4 weeks, immunoblots for frataxin in heart, liver and muscle tissues was performed. (B) Quantification of frataxin levels normalized to GAPDH. (C) Immunohistochemistry of frataxin expression in heart tissue, scale bar=50 μm. (D) AAV9-frataxin or AAV9-NC mice were subjected to I/R injury, and serum LDH levels were then measured. (E) Representative heart slices with TTC staining 4 h after I/R injury. (F) Quantitative analysis of infarct size. (G) Representative M-mode echocardiographic images 1 wk after I/R injury. (H) (I) Quantitative analysis of EF and FS of AAV9-frataxin or AAV0-NC mice following I/R injury. Data are shown as mean ± SEM, n=5. *$P < 0.05$, **$P < 0.01$ vs. AAV9-NC sham; $^{\#}P < 0.05$, $^{\#\#}P < 0.01$ vs. I/R.

Figure 8. Frataxin overexpression inhibited myocardial ferroptosis in vivo.

AAV9-frataxin or AAV9-NC mice were subjected to I/R injury; cardiac *ptgs2* mRNA (A), MDA (B), and iron (C) levels; 4-HNE levels (D, scale bar=20 μm); aconitase activity (E); and TFR, FHC and frataxin (F) levels were measured. In (G), (H) and (I), quantification of FHC, frataxin, and TFR levels, respectively, were normalized to GAPDH. Data are shown as mean ± SEM, n=5. $^{*}P < 0.05$, $^{**}P < 0.01$ vs. AAV9-NC sham; $^{\&\&}P < 0.01$ vs. I/R; I $^{\#}P < 0.05$, $^{\#\#}P < 0.01$ vs. I/R.

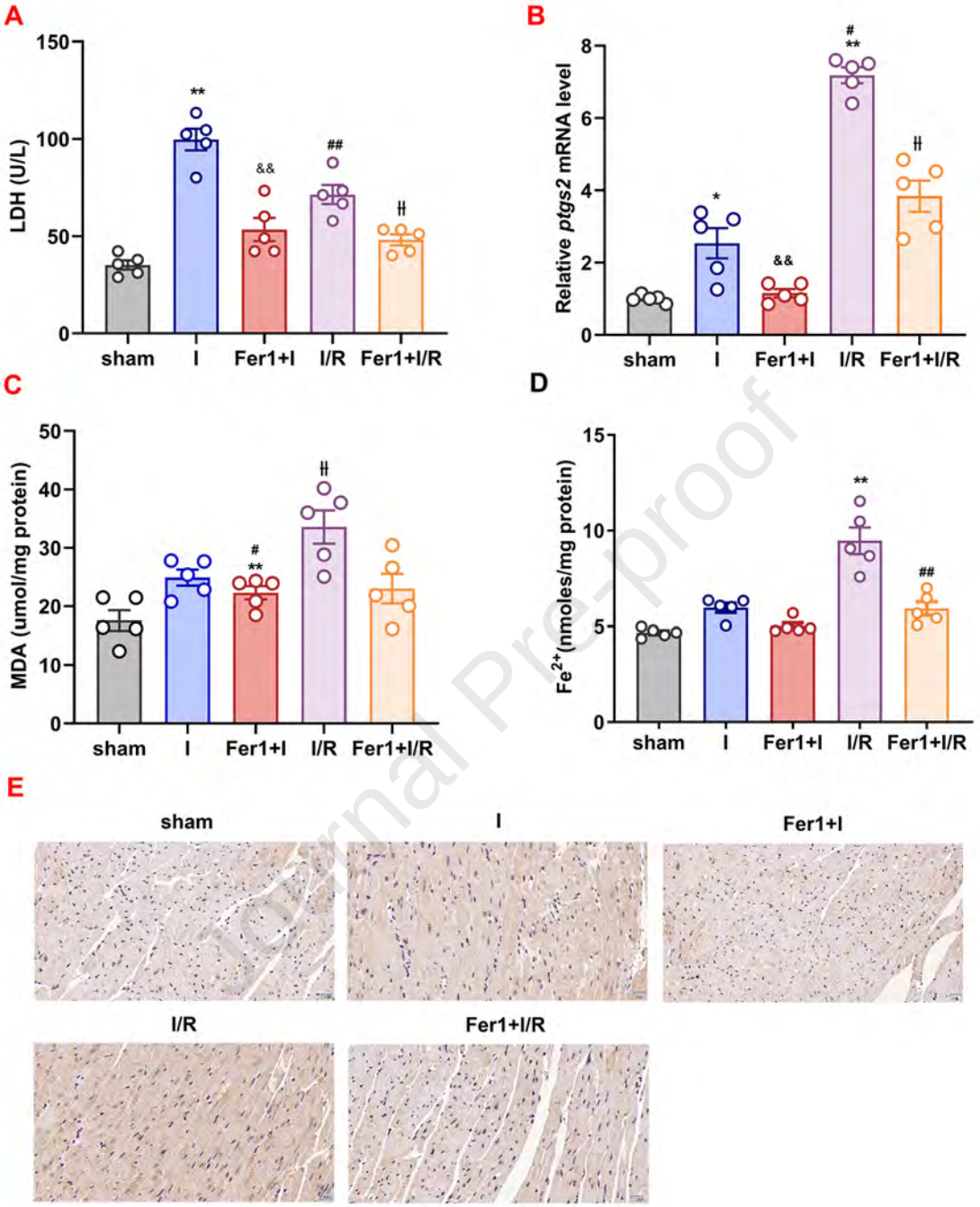

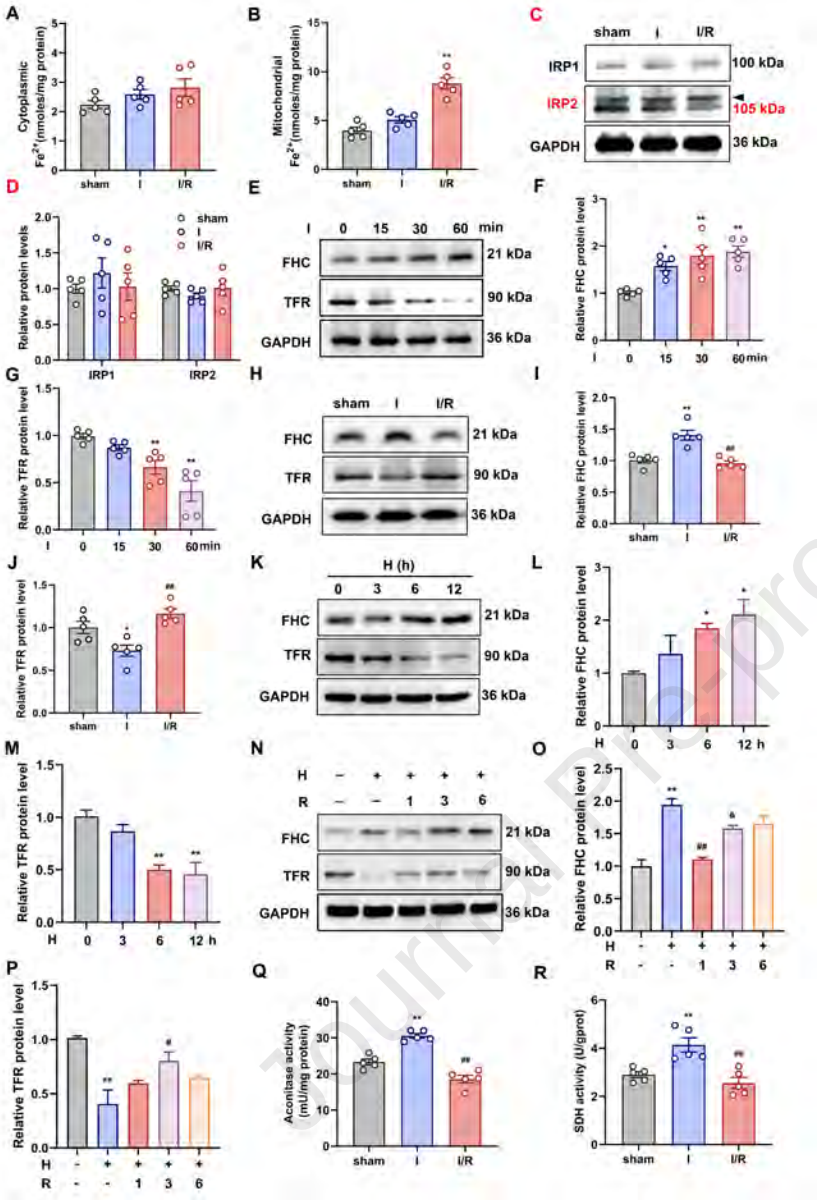

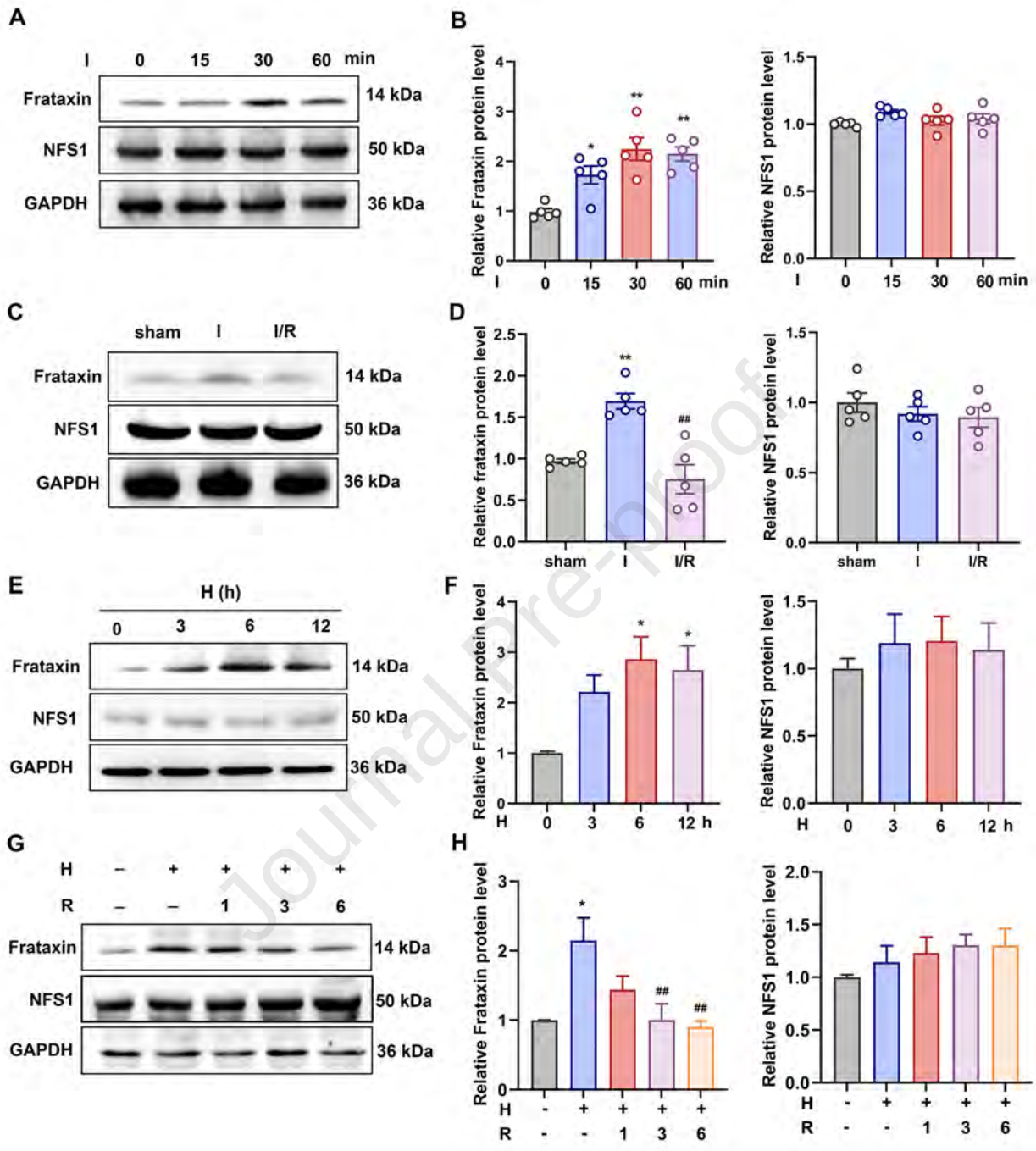

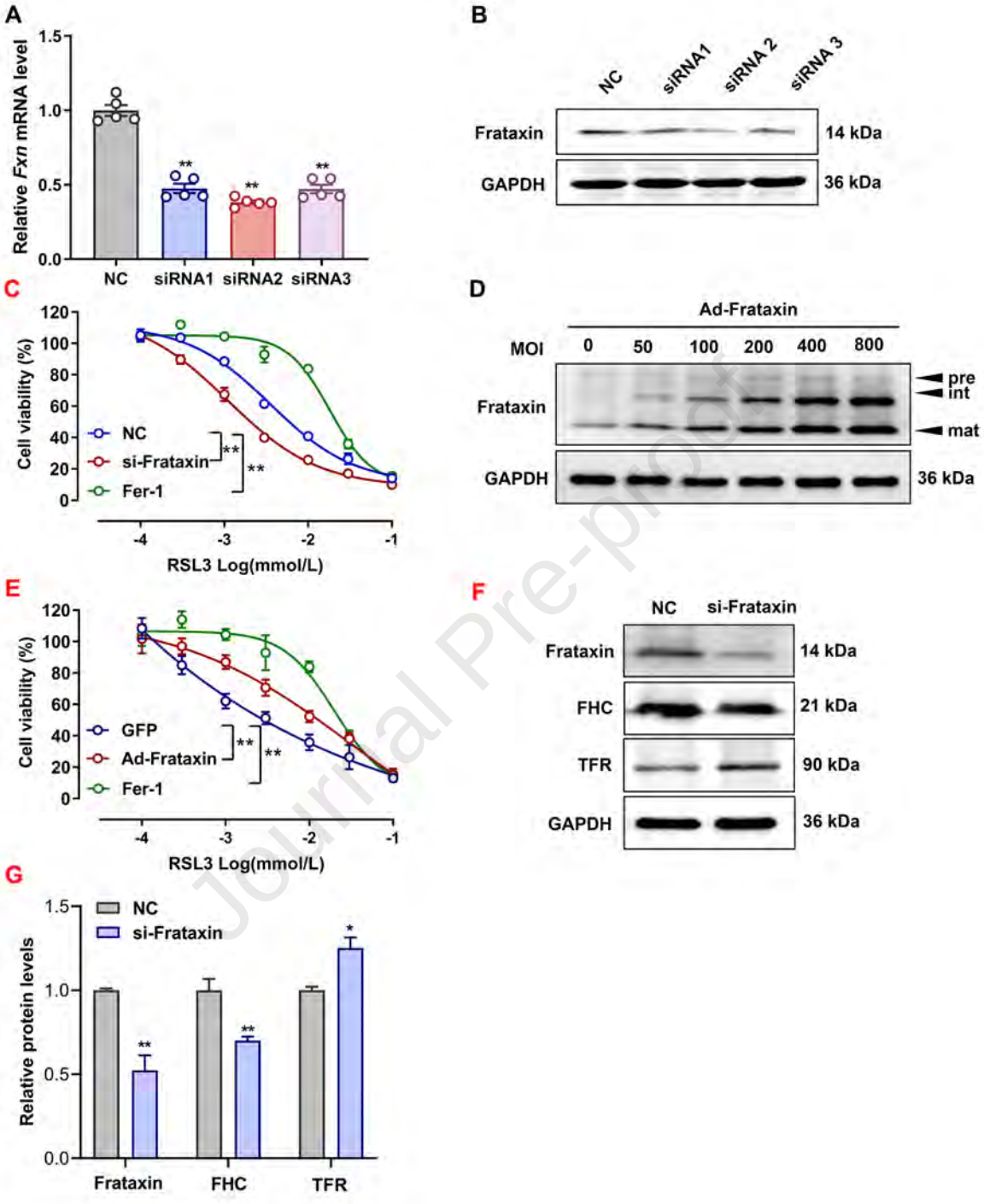

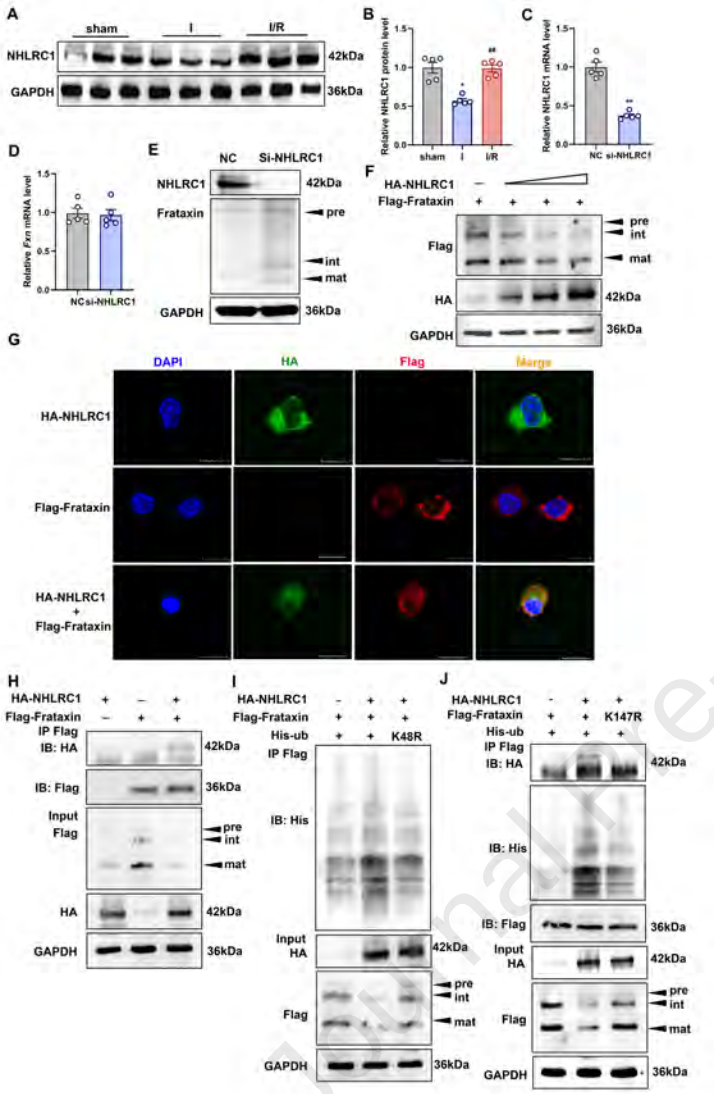
A
sham
I
I/R
NHLRC1
GAPDH
42kDa
36kDa
B
Relative NHLRC1 protein level
sham
I
I/R
C
Relative NHLRC1 mRNA level
NC
si-NHLRC1
D
Relative Fxn mRNA level
NC
si-NHLRC1
E
NC
Si-NHLRC1
NHLRC1
Frataxin
GAPDH
pre
int
mat
F
HA-NHLRC1
Flag-Frataxin
Flag
HA
GAPDH
G
DAPI
HA
Flag
Merge
HA-NHLRC1
Flag-Frataxin
HA-NHLRC1 + Flag-Frataxin
H
IP Flag
IB: HA
IB: Flag
Input Flag
HA
GAPDH
I
His-ub
K48R
IP Flag
IB: His
Input HA
Flag
J
K147R
IP Flag
IB: HA
IB: His
IB: Flag
Input HA
Flag
GAPDH

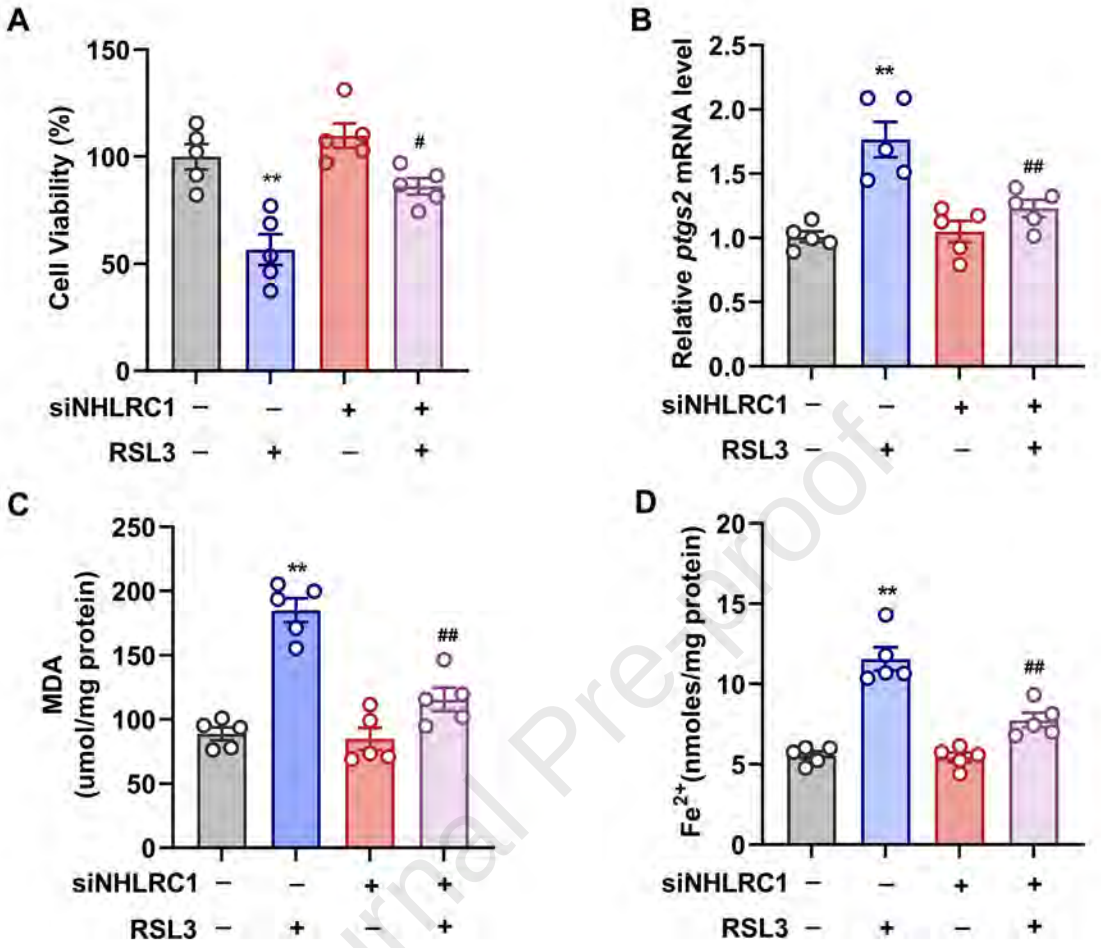

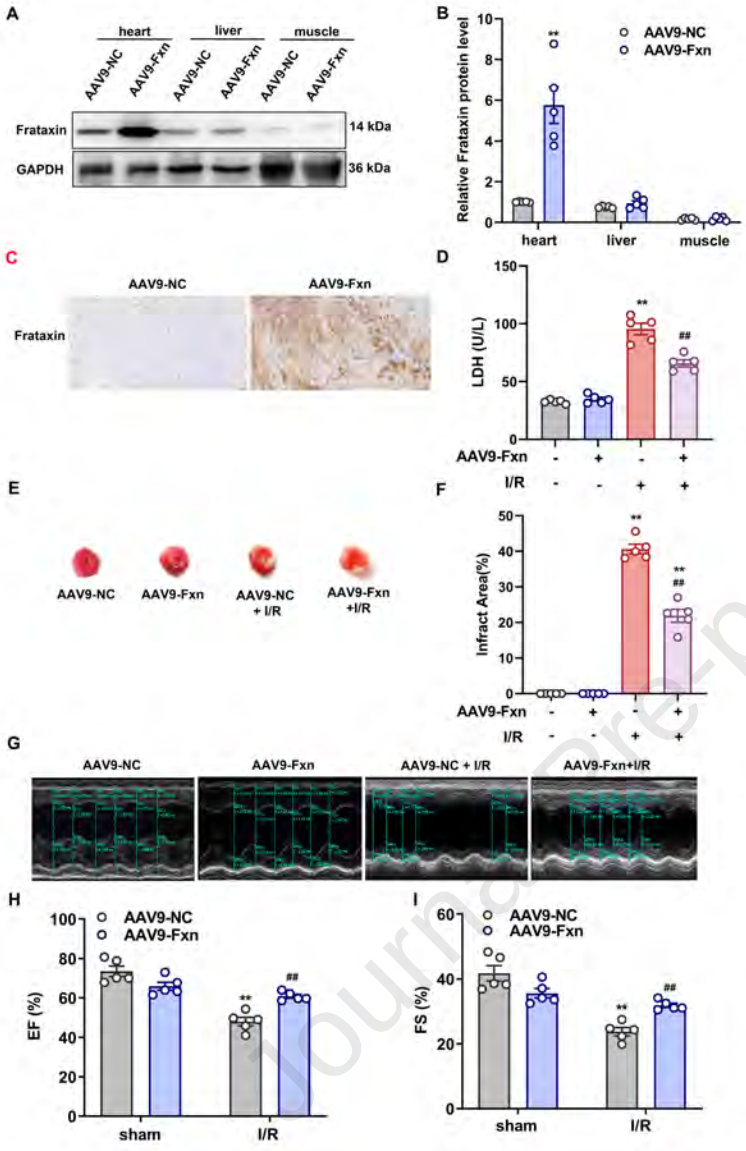
A
heart
liver
muscle
AAV9-NC
AAV9-Fxn
Frataxin
GAPDH
14 kDa
36 kDa
B
Relative Frataxin protein level
AAV9-NC
AAV9-Fxn
heart
liver
muscle
C
AAV9-NC
AAV9-Fxn
Frataxin
D
LDH (U/L)
AAV9-Fxn
I/R
E
AAV9-NC
AAV9-Fxn
AAV9-NC + I/R
AAV9-Fxn +I/R
F
Infract Area(%)
AAV9-Fxn
I/R
G
AAV9-NC
AAV9-Fxn
AAV9-NC + I/R
AAV9-Fxn+I/R
H
EF (%)
AAV9-NC
AAV9-Fxn
sham
I/R
I
FS (%)
AAV9-NC
AAV9-Fxn
sham
I/R

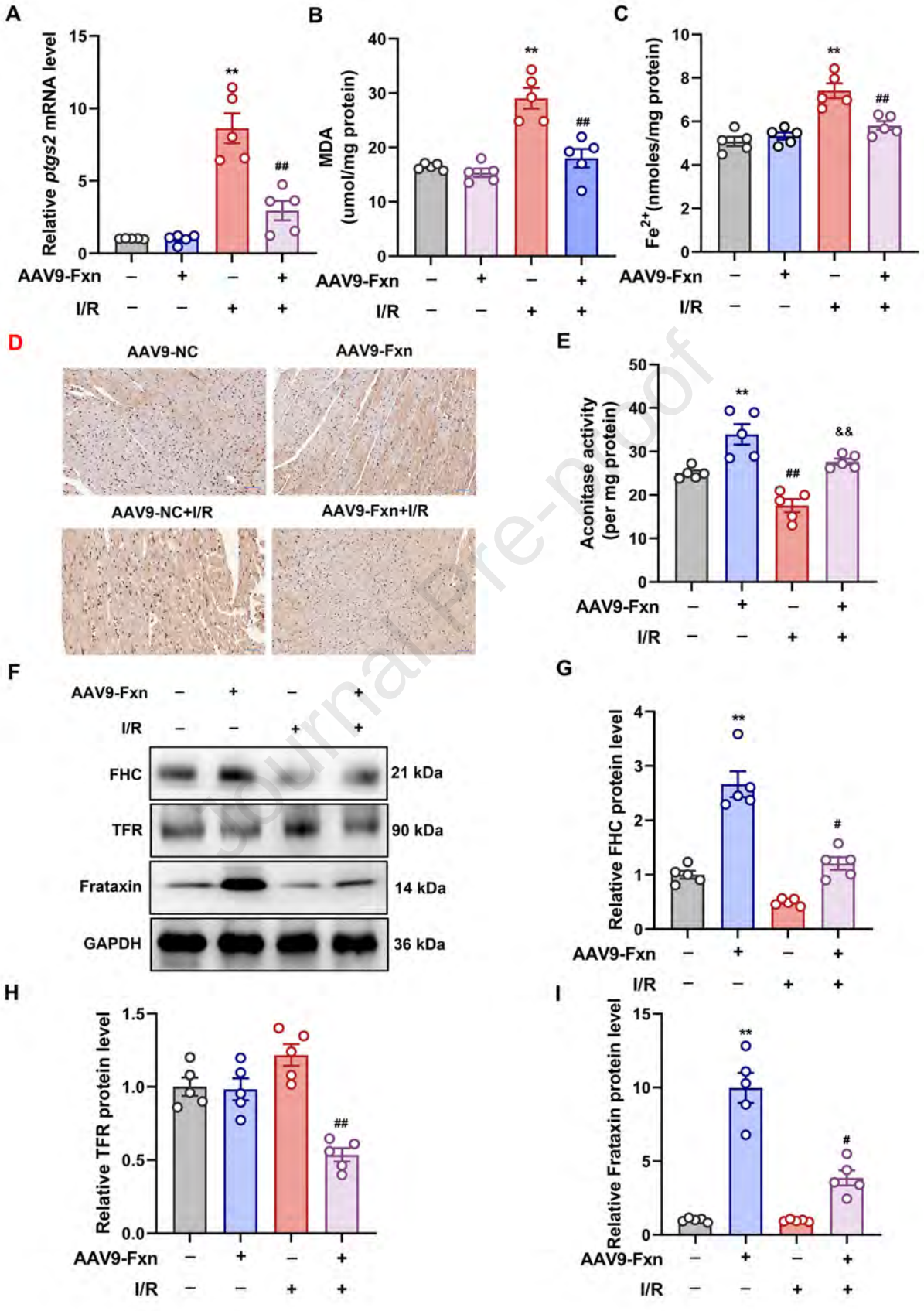

Highlights

- IRP activity was enhanced in ischemic hearts and weakened in reperfused hearts.
- NHLRC1 promoted frataxin ubiquitination and degradation.
- Cardiac-specific frataxin overexpression protected against myocardial I/R injury through ferroptosis inhibition.

Declaration of competing interest

The authors have declared that no competing interest exists.